MAGNETIC FIELD MEASUREMENTS AT AU SCALES AROUND MASSIVE YOUNG STELLAR OBJECTS BY USING ASTRONOMICAL MASERS

Gabriele Surcis
(surcis@jive.nl)

Collaborators:
W.H.T. Vlemmings (Chalmers Uni, Sweden), H.J. van Langevelde (JIVE, Leiden Uni, The Netherlands), B. Hutawarakorn Kramer (MPIfR, Germany), A. Bartkiewicz (Copernicus Uni, Poland), C. Goddi (Radboud Uni, The Netherlands), L. Moscadelli (INAF, Italy), A. Sanna (MPIfR, Germany), J.M. Torrelles (CSIC, Spain), J.-S. Kim (NAOC, Japan), S.-W. Kim (KASI, South Korea), J. Cantó (UNAM, Mexico), S. Curiel (UNAM, Mexico)

Outline

- Introduction

  polarized maser emissions

- The flux-limited sample
- Magnetic field changes in W75N
- Summary & Follow-ups
- New large project

INTRODUCTION: polarized maser emissions

Masers are **bright** and have **narrow spectral lines**

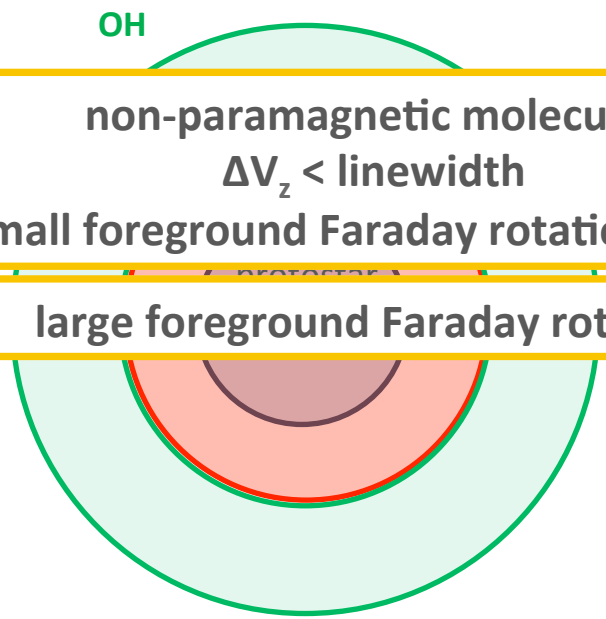

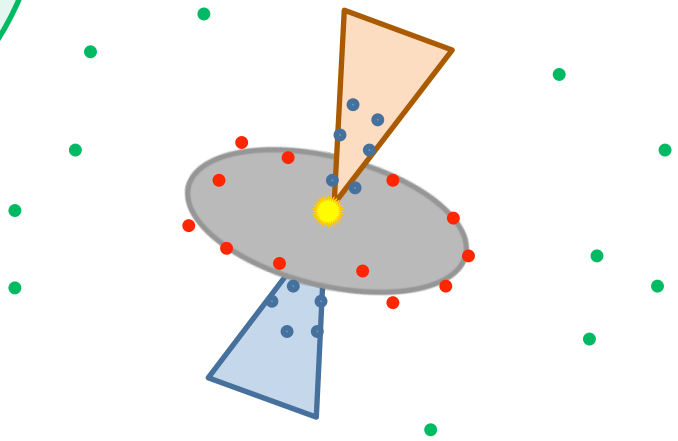

	Frequency (GHz)	Density (cm^{-3})	P_I (%)	P_V (%)
non-paramagnetic molecules ΔV_z < linewidth small foreground Faraday rotation (<10°)	22	$10^8 < n_{H2} < 10^{10}$	<20	<1
	6.7	$10^7 < n_{H2} < 10^9$	<12	<1
large foreground Faraday rotation	1.6/1.7	$n_{H2} < 10^8$	<100	<100

INTRODUCTION: polarized maser emissions

Full radiative transfer method (FRTM)

Nedoluha & Watson 1992, ApJ, 384,185

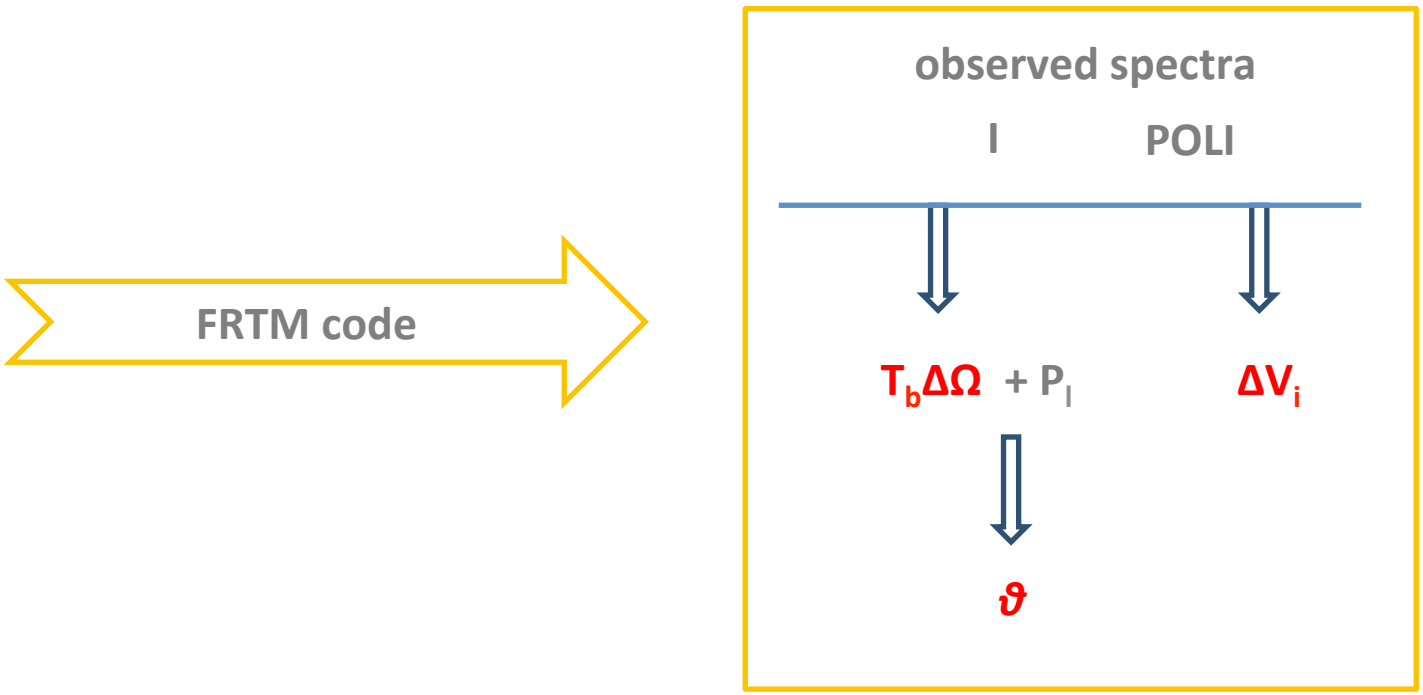

Vlemmings, W.H.T. et al. 2006, A&A, 448, 597

INTRODUCTION: polarized maser emissions

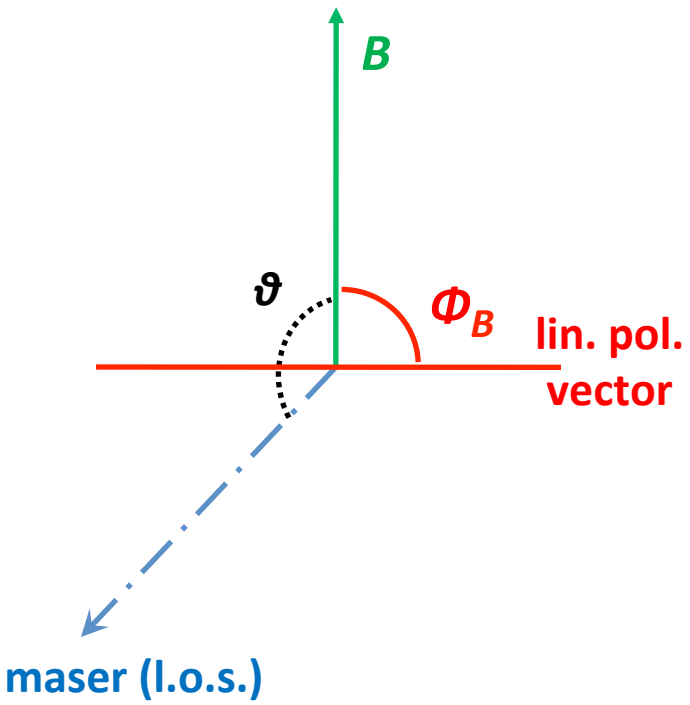

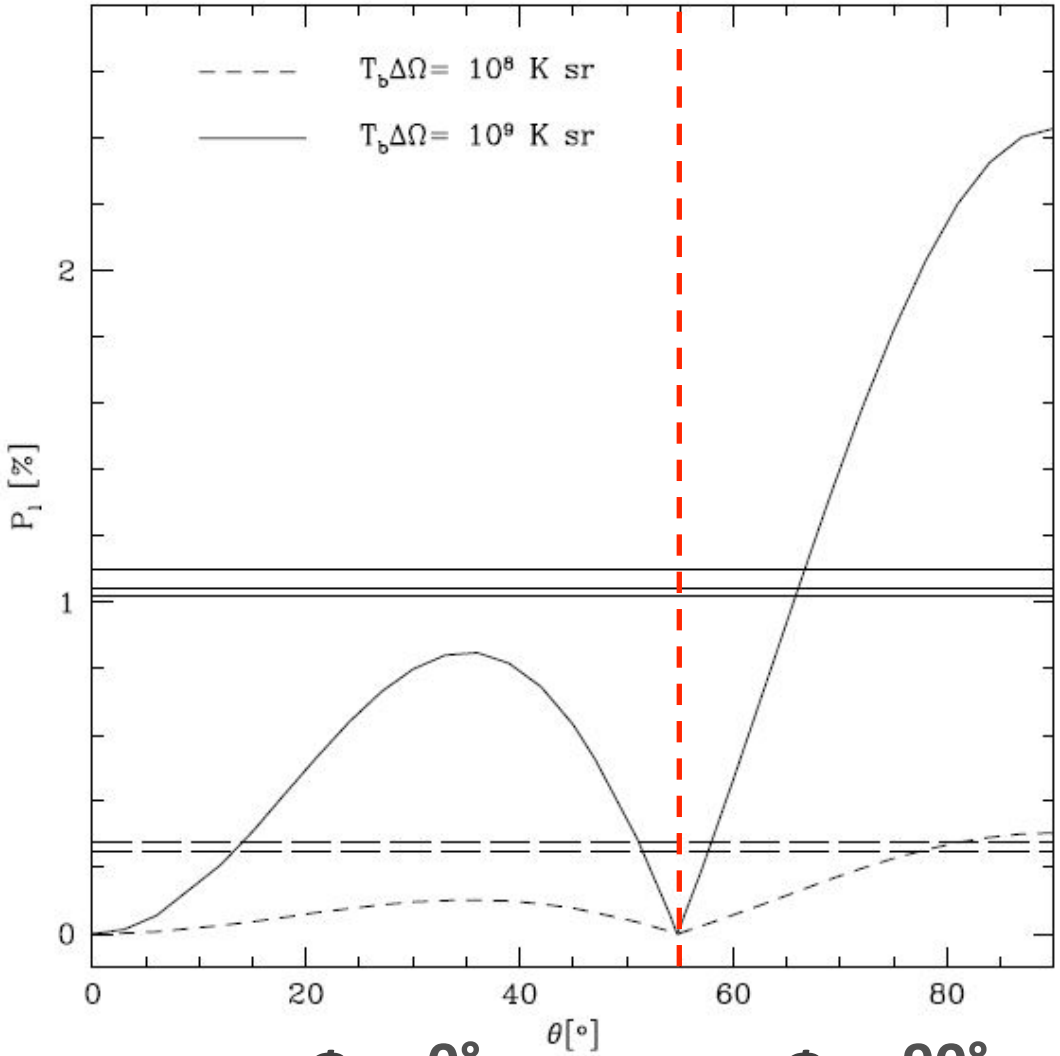

$\Phi_B = 0°$

$\Phi_B = 90°$

Goldreich, P et al. 1973, ApJ, 179, 111

INTRODUCTION: polarized maser emissions

Zeeman splitting & Magnetic field strength

Surcis, G. et al. 2011, A&A, 527, 48

FRTM code + $T_b \Delta\Omega$ + ΔV_i

$B_{||} = B \cdot V_z \cos\vartheta$

$B_{||} = \Delta V_z / \alpha_z$

CH_3OH maser

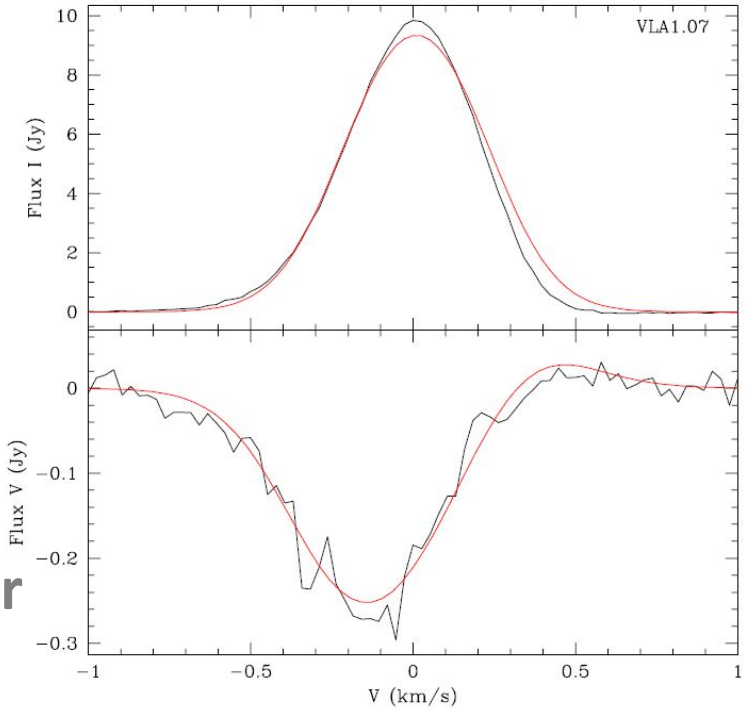

~~unknown~~ g-factors

Lankhaar, B. et al. 2015, in prep.
Vlemmings, W.H.T. et al. 2015, in prep.

Surcis et al. 2015, PoS (EVN 2014) 041, arXiv: 1503.02403

THE FLUX-LIMITED SAMPLE

EUROPEAN VLBI NETWORK (EVN)

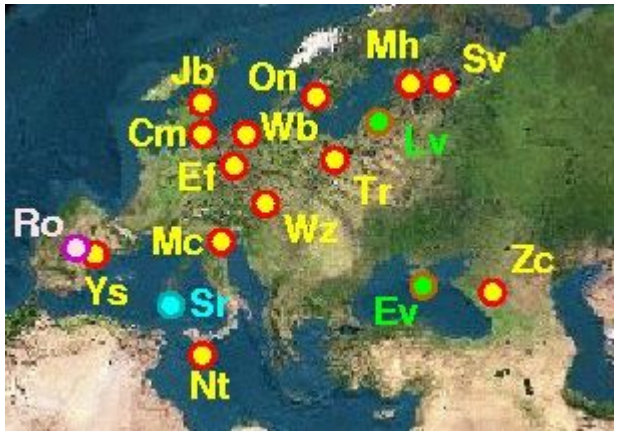

11 massive star-forming regions observed from 2008 to 2011

Frequency: 6.6679 GHz (CH_3OH masers)

Angular resolution: 0''.001

Surcis et al. 2009, A&A, 506, 757
Surcis et al. 2011, A&A, 533, 47
Surcis et al. 2012, A&A, 541, 47
Surcis et al. 2013, A&A, 556, 73

Flux limited sample (total = 133 hours)

Pestalozzi et al (2005): catalogue of 6.7-GHz methanol masers
Declination > -9°; $Flux_{single\text{-}dish}$ > 50 Jy (total number of sources = 31)

+ 19 massive star-forming regions remain to be observed
Observations from November 2012 to June 2015

Results of the first 7 sources ⟹ *Surcis et al. 2015, A&A, submitted*

THE FLUX-LIMITED SAMPLE

*Surcis, G. et al. 2009, 2011, 2012, 2013, 2014, 2015**

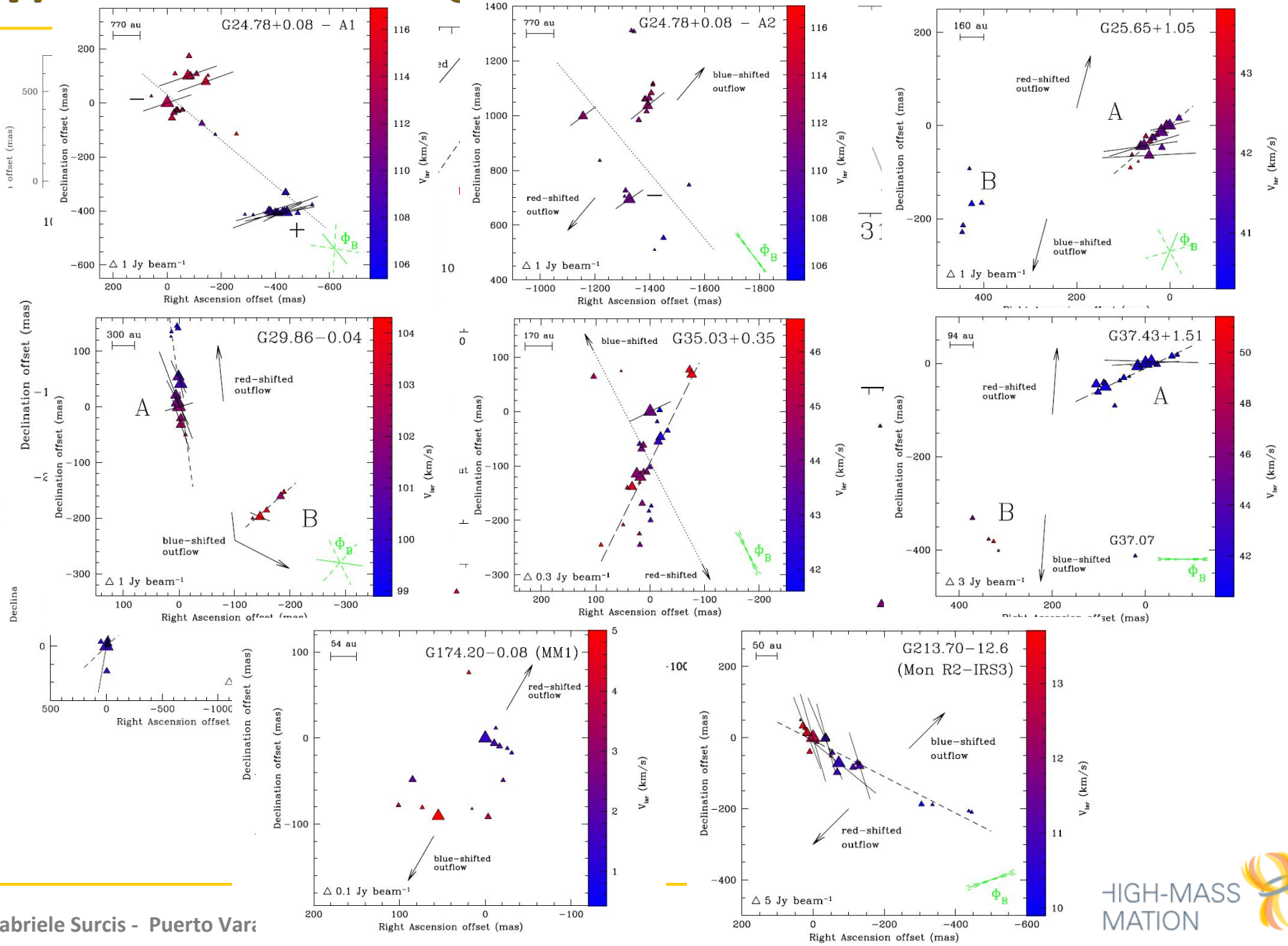

HIGH-MASS MATION

THE FLUX-LIMITED SAMPLE

flux limited sample + southern sources (Dodson & Moriarty 2012)

Table 2. Comparison between position angle of magnetic field, CH_3OH maser distribution, outflows, and linear polarization angles.

(1) Source	(2) $\langle\chi\rangle$ (°)	(3) $\langle\Phi_B\rangle$ (°)	(4) $PA_{outflow}$ (°)	(5) PA_{CH_3OH} (°)	(6) ρ	(7) $\lvert PA_{outflow} - \langle\Phi_B\rangle\rvert$ (°)	(8) $\lvert PA_{CH_3OH} - \langle\chi\rangle\rvert$ (°)	(9) $\lvert PA_{CH_3OH} - PA_{outflow}\rvert$ (°)	(10) ref.[a]
IRAS 20126+4104	−70 ± 16	+20 ± 16	−65 ± 5[b]	+87 ± 4	+0.12	85 ± 17	23 ± 17[c]	28 ± 6[c]	(1), (2)
G24.78+0.08-A2	−53 ± 2	+37 ± 2[d]	−40 ± 15[e]	−26 ± 19	-0.77	77 ± 15	79 ± 19	66 ± 24	(3), (4)
G25.65+1.05	−80 ± 8	−23 ± 51[d]	−15 ± 15[e]	−49 ± 7[f]	-0.87	8 ± 53	31 ± 11	64 ± 17	(3), (5)
G29.86-0.04	+46 ± 41	+82 ± 56[d]	+6 ± 15[e,g]	+8 ± 7[f]	+0.73	76 ± 58	38 ± 42	14 ± 17	(3), (6)
G35.03+0.35	−64 ± 5	+26 ± 5[d]	+27 ± 15[e,h]	−26 ± 19	-0.77	1 ± 16	38 ± 20	53 ± 24	(3), (7), (8)
G37.43+1.51	+90 ± 3	+90 ± 3[d]	−4 ± 15[e]	−64 ± 5[f]	-0.87	86 ± 15[c]	26 ± 6[c]	60 ± 16	(3), (9)
G174.20-0.08	–	–	−40 ± 15[e]	−63 ± 16	-0.45	–	–	23 ± 22	(3), (10)
G213.70-12.6	+20 ± 5	−70 ± 5[d]	−45 ± 15[e]	+63 ± 2	+0.95	25 ± 16	43 ± 5	72 ± 15[c]	(3), (11)
From Paper II[i].									
Cepheus A	−57 ± 28	+30 ± 19	+40 ± 4	−79 ± 9	-0.34	10 ± 19	22 ± 29	61 ± 10	(12)
W75N-group A	−13 ± 9	+77 ± 9	+66 ± 15	+43 ± 10	+0.96	11 ± 18	56 ± 14	23 ± 18	(12)
NGC7538-IRS1	−30 ± 69	+67 ± 70	−40 ± 10	+84 ± 7	+0.15	73 ± 71	66 ± 69	56 ± 12	(12)
W3(OH)-group II	+21 ± 45	−47 ± 44	–	−59 ± 6	-0.84	–	80 ± 45	–	(12)
W51-e2	+33 ± 16	−60 ± 21	−50 ± 20	+57 ± 8	+0.70	10 ± 29	24 ± 18	73 ± 22	(12)
IRAS18556+0138	−2 ± 11	+88 ± 11	+58 ± 23	−40 ± 2	-0.99	30 ± 26	42 ± 11	82 ± 23	(12)
W48	+23 ± 7	−67 ± 7	–	+55 ± 10	+0.70	–	78 ± 12	–	(12)
IRAS06058+2138-NIRS1	+49 ± 47	−49 ± 52	−50 ± 15	+78 ± 7	+0.64	1 ± 54	29 ± 48	52 ± 17	(12)
IRAS22272+6358A	−80 ± 15	+9 ± 15	−40 ± 15	−35 ± 11	-0.87	49 ± 21	45 ± 19	5 ± 19	(12)
S255-IR	+36 ± 12	−54 ± 12	+75 ± 15	−63 ± 49	-0.11	51 ± 19	81 ± 51	42 ± 51	(12)
S231	+28 ± 49	−62 ± 49	−47 ± 5	+28 ± 8	+0.97	15 ± 49	0 ± 50	75 ± 9	(12)
G291.27-0.70	−32 ± 5	+52 ± 5	–	−77 ± 14	–	–	45 ± 15	–	(12)
G305.21+0.21	−51 ± 14	28 ± 14	–	+48 ± 23	–	–	81 ± 27	–	(12)
G309.92+0.47	+2 ± 56	−75 ± 56	–	+35 ± 5	–	–	33 ± 56	–	(12)
G316.64-0.08	−67 ± 36	+21 ± 36	–	+34 ± 29	–	–	79 ± 46	–	(12)
G335.79+0.17	+44 ± 28	−41 ± 28	–	−69 ± 25	–	–	67 ± 38	–	(12)
G339.88-1.26	+77 ± 24	−12 ± 24	–	−60 ± 17	–	–	43 ± 29	–	(12)
G345.01+1.79	+5 ± 39	−86 ± 39	–	+74 ± 4	–	–	69 ± 39	–	(12)
NGC6334F (central)	+77 ± 20	−13 ± 20	+30 ± 15[e]	−41 ± 16	–	43 ± 25	62 ± 26	71 ± 41	(12); (13)
NGC6334F (NW)	−71 ± 20	+19 ± 20	+30 ± 15[e]	−80 ± 38	–	11 ± 25	9 ± 43	70 ± 41[c]	(12); (13)

Surcis et al. 2015, A&A, submitted

Paper II : Surcis et al. 2013, A&A, 556,73

THE FLUX-LIMITED SAMPLE

Preliminary result:
Magnetic field oriented along the large scale molecular outflows

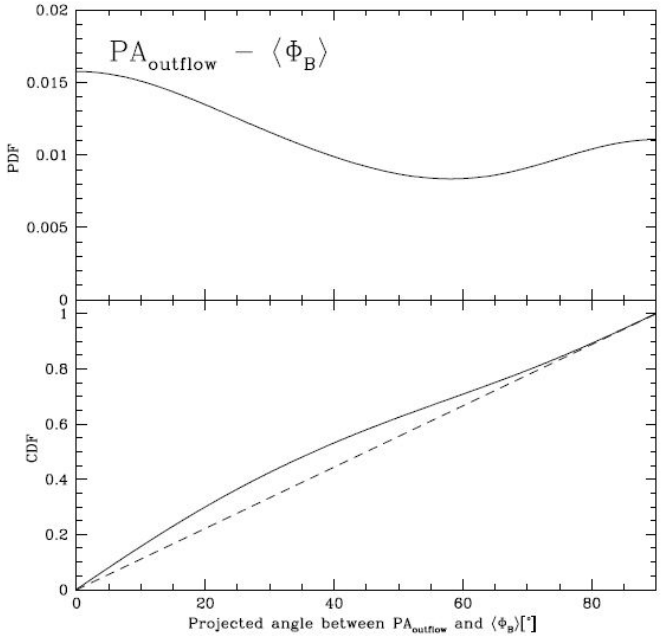

Fig. 10. The probability distribution function (PDF, top panel) and the cumulative distribution function (CDF, bottom panel) of the projected angle between the magnetic field and the outflow axes ($|PA_{outflow} - \langle\Phi_B\rangle|$). The dashed line is the CDF for random orientation of outflows and magnetic fields, i.e. all angular differences are equally likely. The results of the Kolmogorov-Smirnov test can be found in Table 3

Table 3. Results of Kolmogorov-Smirnov test.

(1) Angle	(2) N	(3) D^a	(4) λ^b	(5) $Q_{K-S}(\lambda)^c$
$\lvert PA_{CH_3OH} - \langle\chi\rangle\rvert$	27	0.12	0.65	0.79
$\lvert PA_{CH_3OH} - PA_{outflow}\rvert$	19	0.26	1.18	0.12
$\lvert PA_{outflow} - \langle\Phi_B\rangle\rvert$	18	0.28	1.22	0.10

Probability that the angles are drawn from random distribution

$$Q_{K-S}(\lambda) = 2\sum_{j=1}^{N}(-1)^{j-1}e^{-2j^2\lambda^2}$$

10%

$$\lambda = (\sqrt{N} + 0.12 + 0.11/\sqrt{N}) \times D$$

Surcis et al. 2015, A&A, submitted

MAGNETIC FIELD CHANGES IN W75N(B)

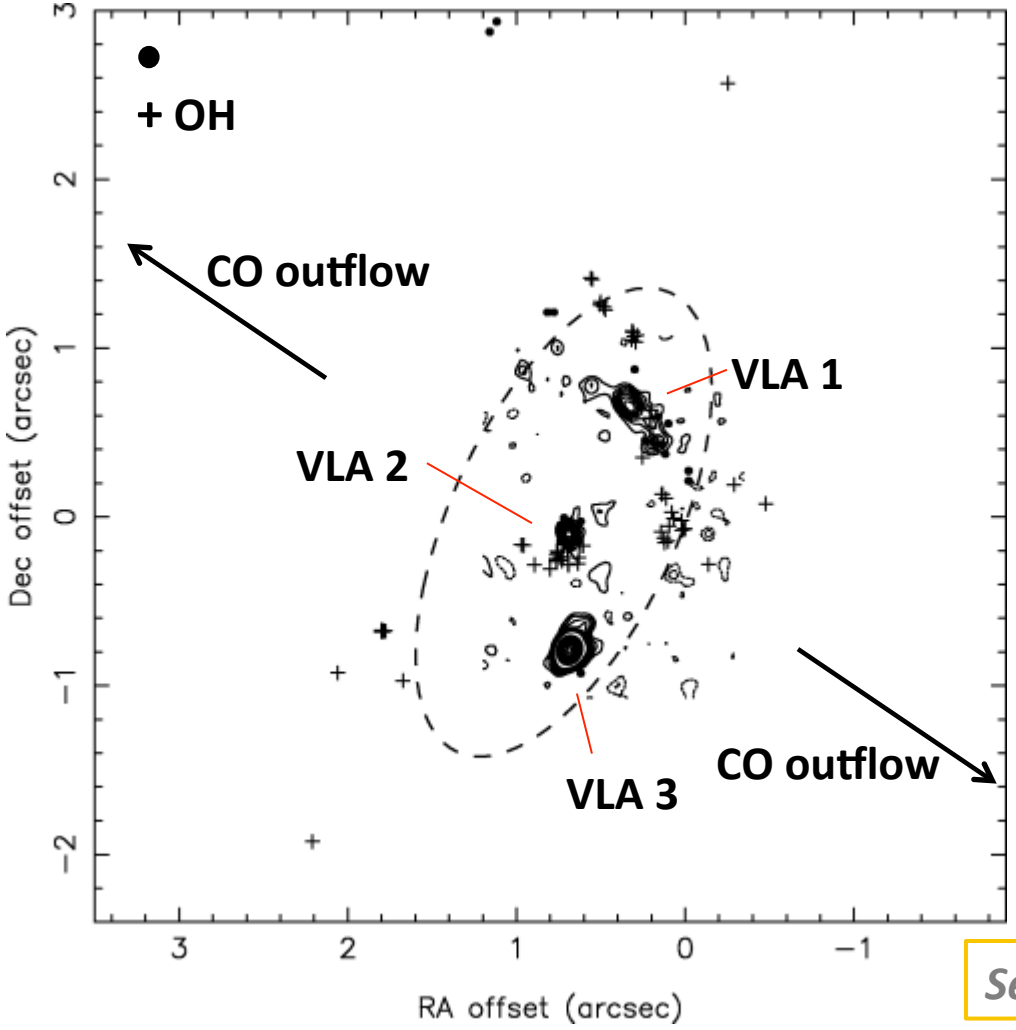

D = 1.3 kpc

Ring radius = 0.015 pc

Separation between VLA1 and VLA2 = 1300 AU

H_2O polarimetric observations:
epochs 2005.89
2012.54

See J.-S. Kim's talk on Thursday @ 11:50

Torrelles et al., 1997, ApJ, 489, 744; Hutawarakorn et al, 2002, MNRAS, 330, 349; e.g. Shepherd et al., 2003, ApJ, 584, 882

MAGNETIC FIELD CHANGES IN W75N(B)

Surcis, G.et al. 2011, A&A, 527, 48

$\overline{|B_{\parallel}|}^{2005.89}_{\rm VLA2} = 345$ mG

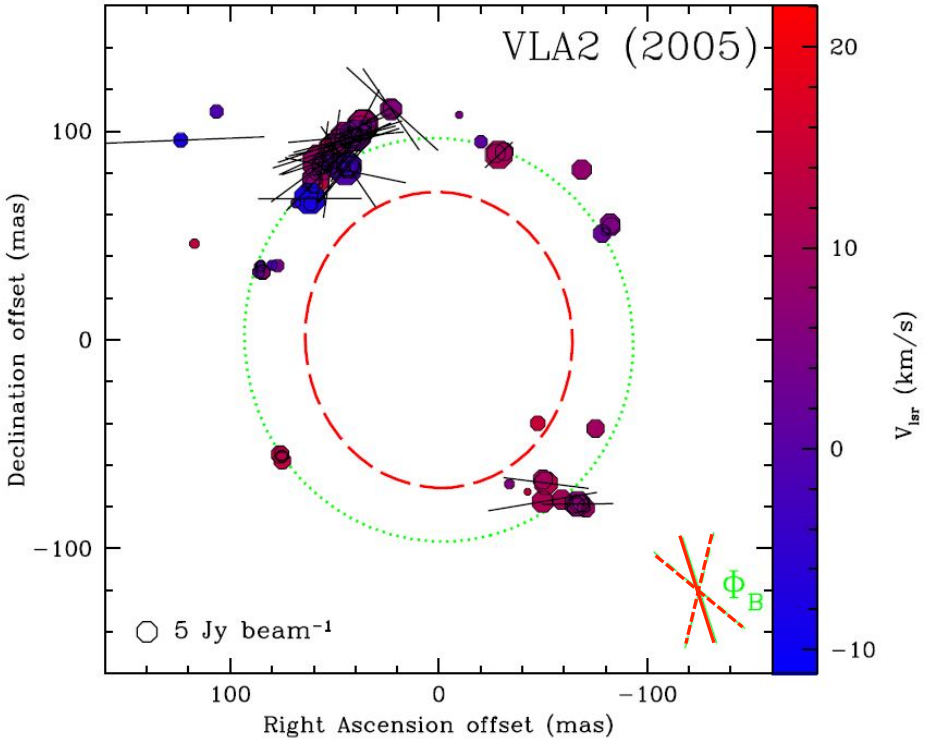

Surcis, G.et al. 2014, A&A, 565, L8

$\overline{|B_{\parallel}|}^{2012.54}_{\rm VLA2} = 128$ mG

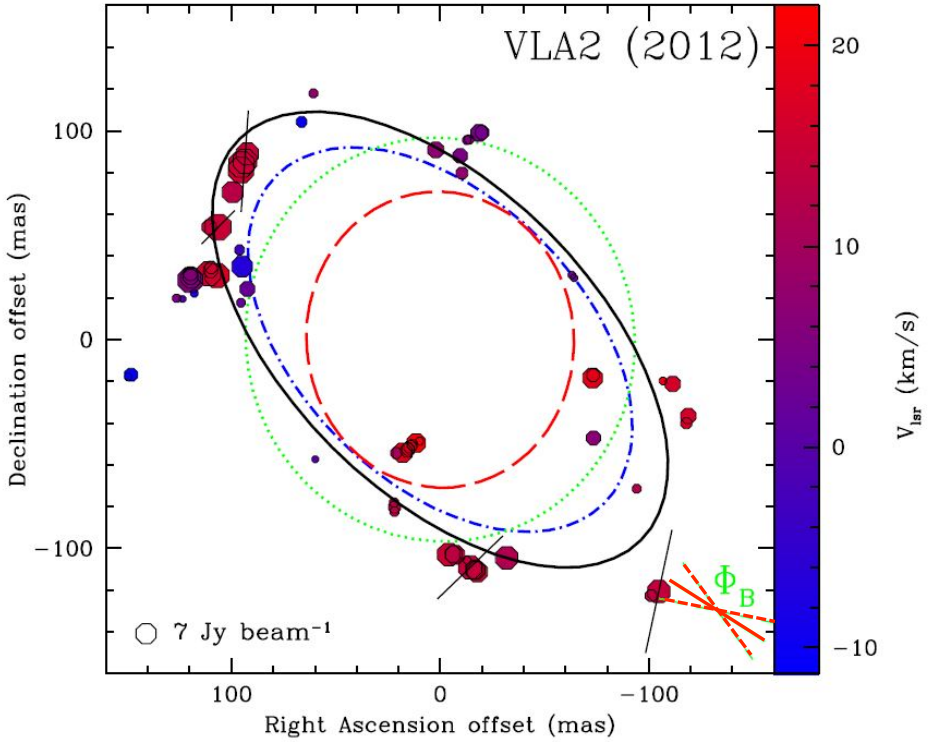

*See **J.-S. Kim**'s talk on **Thursday @ 11:50***

MAGNETIC FIELD CHANGES IN W75N(B)

Surcis, G.et al. 2011, A&A, 527, 48

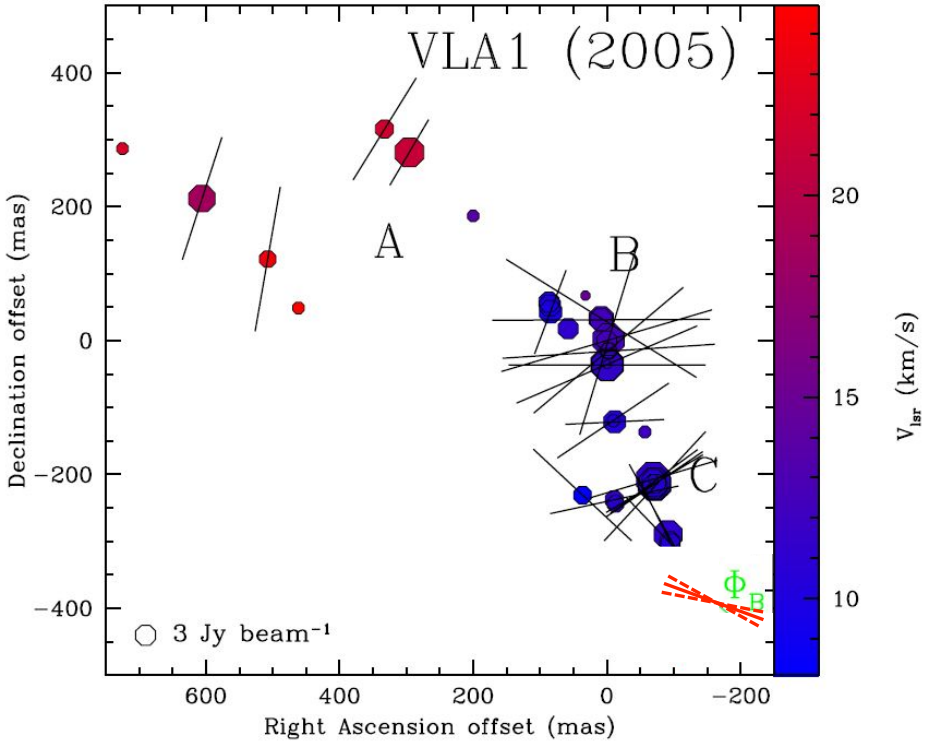

Surcis, G.et al. 2014, A&A, 565, L8

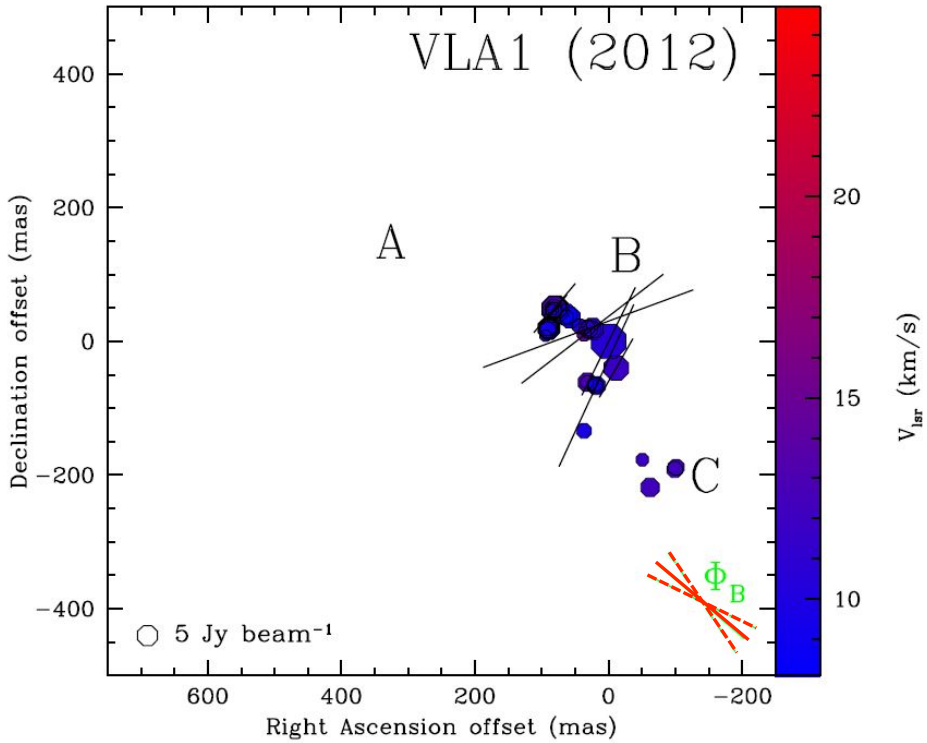

*See **J.-S. Kim's** talk on **Thursday @ 11:50***

MAGNETIC FIELD CHANGES IN W75N(B)

Surcis, G.et al. 2014, A&A, 565, L8

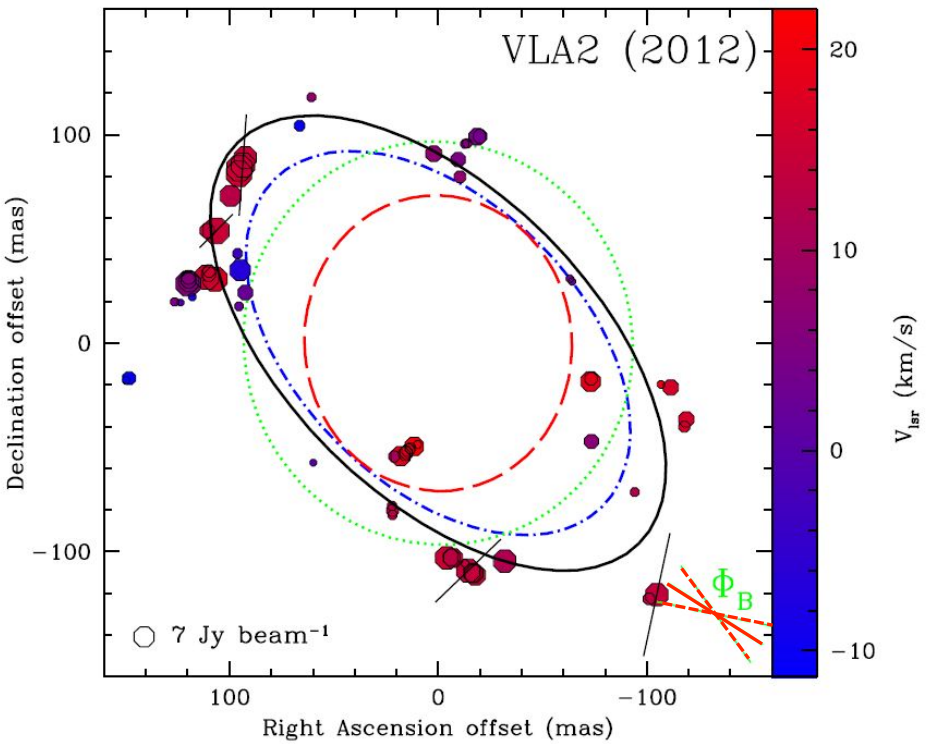

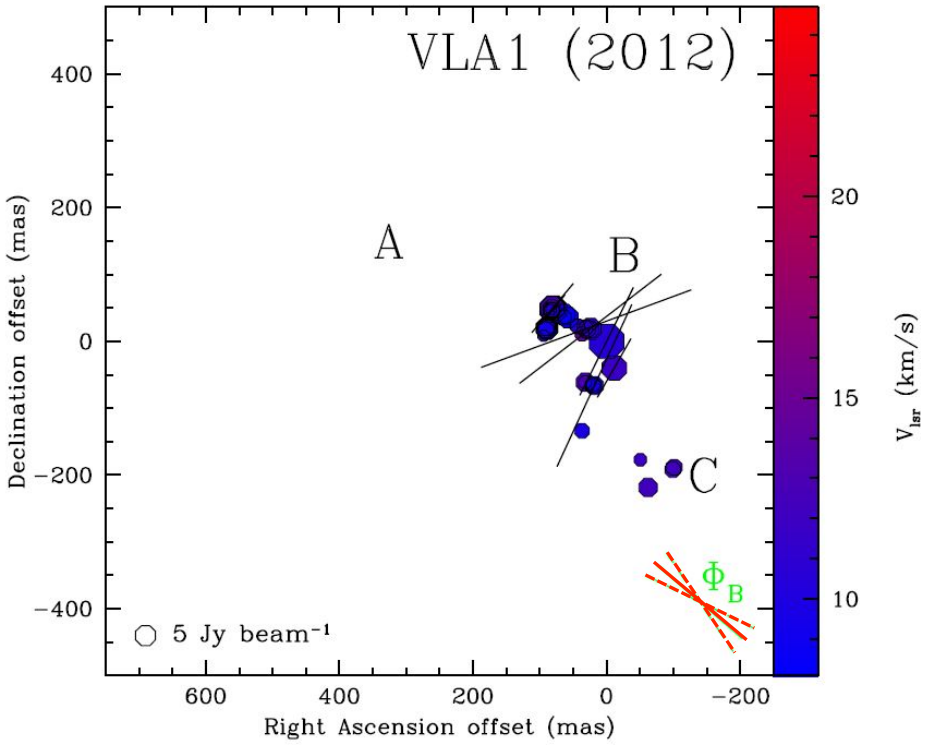

*See **J.-S. Kim's** talk on **Thursday @ 11:50***

SUMMARY

- From CH_3OH masers we found that the probability that **magnetic fields are aligned with the large-scale outflows in massive YSO** may be significant

- **The magnetic field** around W75N(B)-VLA2 has **changed its orientation** according to the new direction of the major-axis of the maser distribution and it is aligned with the magnetic field in W75N(B)-VLA1.

- **Consistency between magnetic field morphology from small to large scale** (e.g., IRAS20126+4104 *Surcis, G. et al. 2014, A&A, 563, 30*)

FOLLOW-UPS

- To reduce and analyse the **remaining sources of the flux-limited sample** (12 massive YSOs)
- **Monitoring project of** the H_2O masers in **W75N(B) over 6 years** (4 epochs spaced by 2 years) with the EVN in full polarization mode. **First epoch observed on 17th June 2014**.
- Finally provide the **magnetic field strength** using the Zeeman-splitting of **CH_3OH** maser ⟹ the **g-factors have just been calculated**

- **e-MERLIN 'Feedback in Massive Star Formation' legacy project**: deep simultaneous continuum and maser polarization observations.
  ⟹ **see Daria Dall'Olio's poster (n. 12)**
- Measuring Magnetic Fields Near and Far with the **SKA** via the Zeeman Effect (*Robishaw, T., Green, J.A., Surcis, G., Vlemmings, W.H.T. et al. 2015 arXiV: 1503.01779*). **Maser polarimetric observations in High-mass star-forming regions.**

NEW LARGE PROJECT

- **GOAL**: To investigate if there exists a **correlation between 3-D maser kinematics and 3-D magnetic field** configuration in a sample of **22 high-mass YSOs**.
- **Around disks** by using CH_3OH maser emission **and along outflows** using H_2O maser emission.

LARGE EVN PROPOSAL – TOTAL TIME = 648 hr

PI:
L. Moscadelli (INAF, Italy),
Co-I:
G. Surcis (JIVE, The Netherlands), P. Hofner (New Mexico Tech, USA), A. Sanna (MPIfR, Germany), C. Goddi (Radboud Uni, The Netherlands), V. Rosero (New Mexico Tech, USA), R. Cesaroni (INAF, Italy), F. Bacciotti (INAF, Italy)

- **Multi epoch polarimetric observations of 6.7 GHz CH_3OH maser emission** to determine the morphology of magnetic field and to measure the proper motion of the masers around protostellar disks.
- **Single epoch of polarimetric observations of 22 GHz H_2O maser** to determine the morphology of magnetic field along the outflows.

THANK YOU

EXTRA SLIDE 1

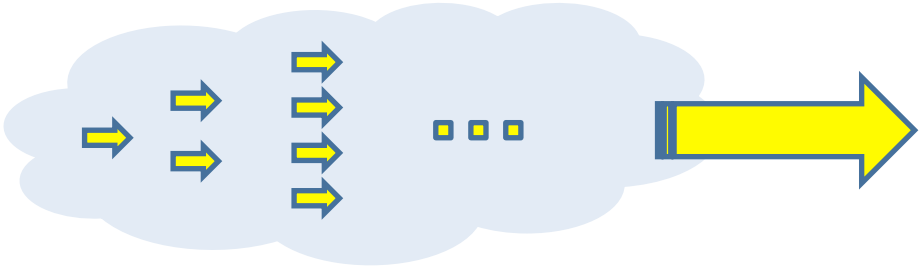

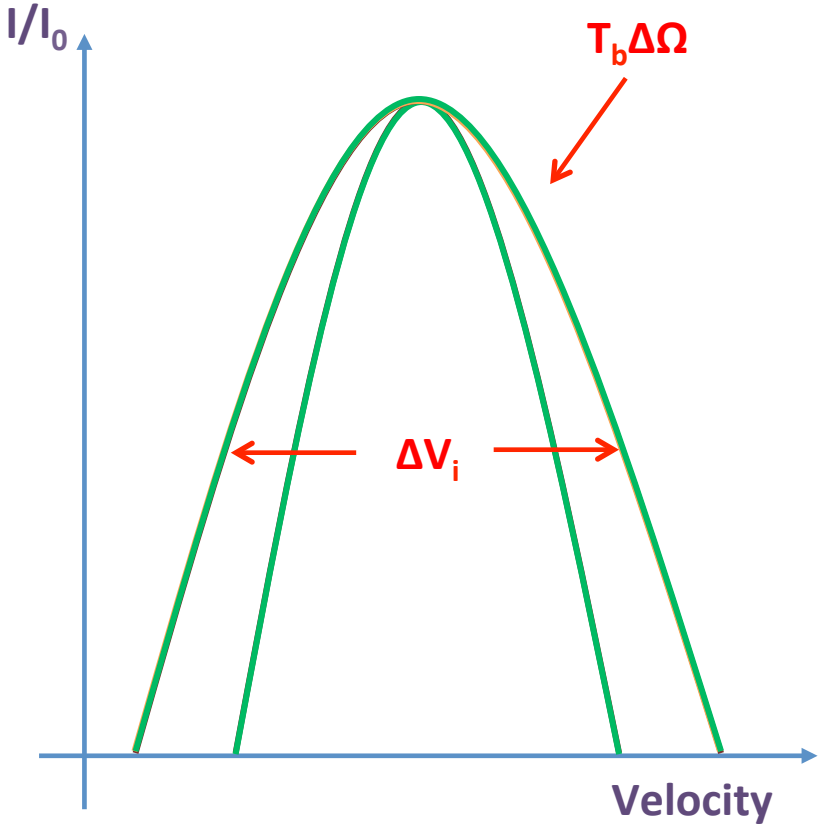

Intrinsic thermal linewidth (ΔV_i)

Emerging brightness temperature ($T_b \Delta\Omega$)

- **Unsaturated masers**

  Stimulated emission rate << Decay rate

  maser grows exponentially

- **Saturated masers**

  Stimulated emission rate >> Decay rate

  maser grows linearly

EXTRA SLIDE 2

$$\Delta V_Z = (10^4\, g\, \mu_N\, M_J) \cdot B_{||}$$

α_Z

$\mu_N = e\hbar / 2 m_n c$

= nuclear magneton

M_J = magnetic quantum number for the rotational transition

EXTRA SLIDE 3

	Obs. Date	observed	correlated	analysed
G24.78+0.08	May 2013	√	√	√
G25.65+1.05	May 2013	√	√	√
G29.86-0.04	June 2013	√	√	√
G35.03+0.35	Nov. 2012	√	√	√
G37.43+1.51	June 2013	√	√	√
G174.20-0.08	Nov. 2012	√	√	√
G213.70-12.6	Nov. 2012	√	√	√
G23.44-0.18	Mar. 2014	√	√	☐
G25.83-0.18	Mar. 2014	√	√	☐
G25.71-0.04	Mar. 2014	√	√	☐
G28.31-0.39	June 2014	√	√	☐
G28.83-0.25	June 2014	√	√	☐
G29.95-0.02	June 2014	√	√	☐
G30.70-0.07	Oct. 2014	√	√	☐
G30.76-0.05	Oct. 2014	√	√	☐
G31.28+0.06	June 2015 (?)	☐	☐	☐
G32.03+0.06	June 2015 (?)	☐	☐	☐
G43.80-0.13	June 2014	√	√	☐
G69.52-0.97	June 2015 (?)	☐	☐	☐

Surcis et al. 2015, A&A, accepted

EXTRA SLIDE 4: IRAS 20126+4104

B0.5 with a mass ~7 M_{sun} **D = 1.64 ± 0.5 kpc** **Δ = CH_3OH maser** **O = H_2O maser**

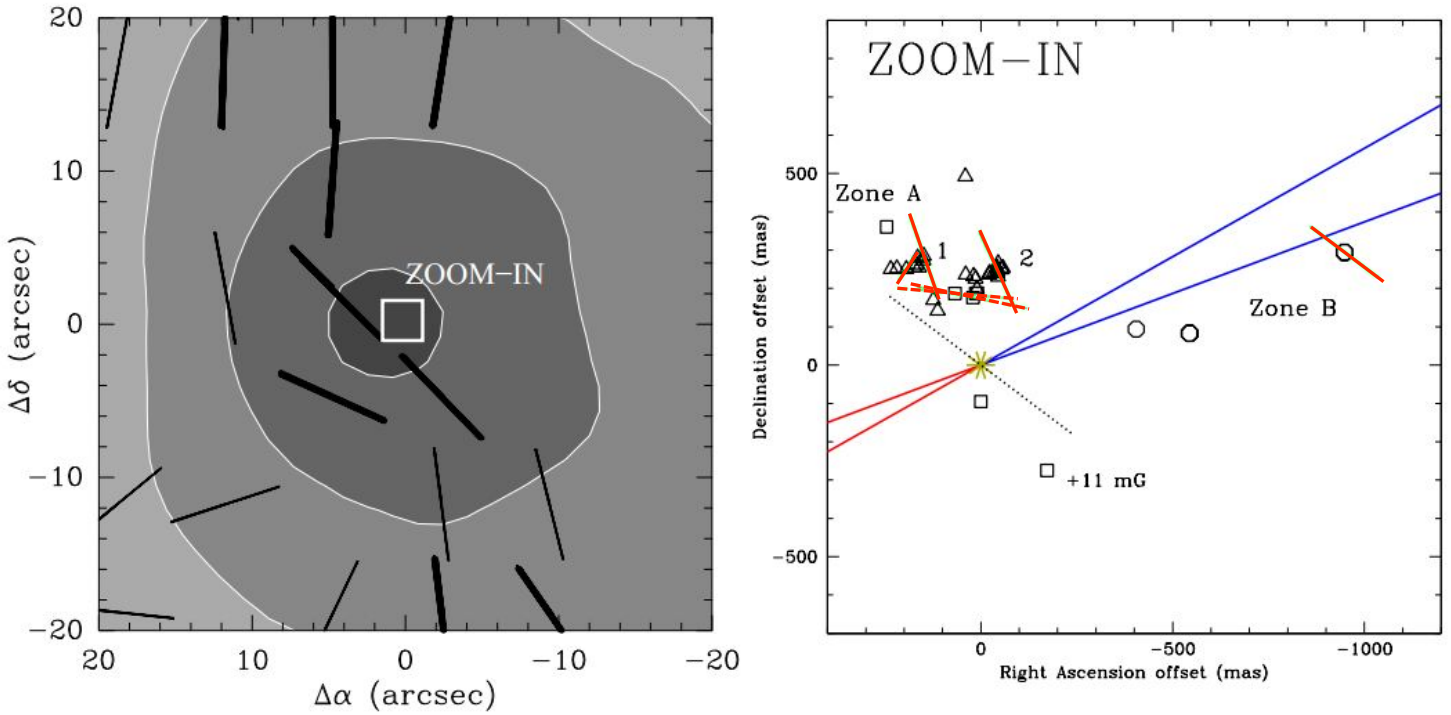

Fig. 4. Left panel: modified version of Fig. 3(b) of Shinnaga et al. (2012). The white box indicates the position of the right panel. The black bars represent the magnetic field direction determined from the polarized dust emission at 350 μm, whose continuum emission is in the background. Right panel: CH_3OH (triangles), OH (squares) (Edris et al. 2005), and H_2O (octagons) masers in IRAS20126+4104. The gold asterisk represents the B0.5 protostar (α_{2000} = $20^h14^m26^s.0498$ and δ_{2000} = 41°13′32″.443, MCR11), while the dotted line represents the Keplerian disk of ~1000 au (PA_{disk} = 53° ± 7°, Cesaroni et al. 2005). The red and blue lines indicate the red- and blue-shifted lobes of the jet, respectively, with a PA_{jet} = 115° and an opening angle of 9° (MCR11). The thick green segments represent the magnetic field direction determined from the polarized CH_3OH and H_2O maser emissions. The green dashed segments represent the magnetic field direction determined from the linearly polarized emission of OH masers (Edris et al. 2005). The foreground Faraday rotation at 1.6-GHz is probably not negligible and needs to be taken into account when interpreting the image (see Sect. 5.2).

Surcis, G. et al. 2014, A&A, 563, 30

EXTRA SLIDE 5

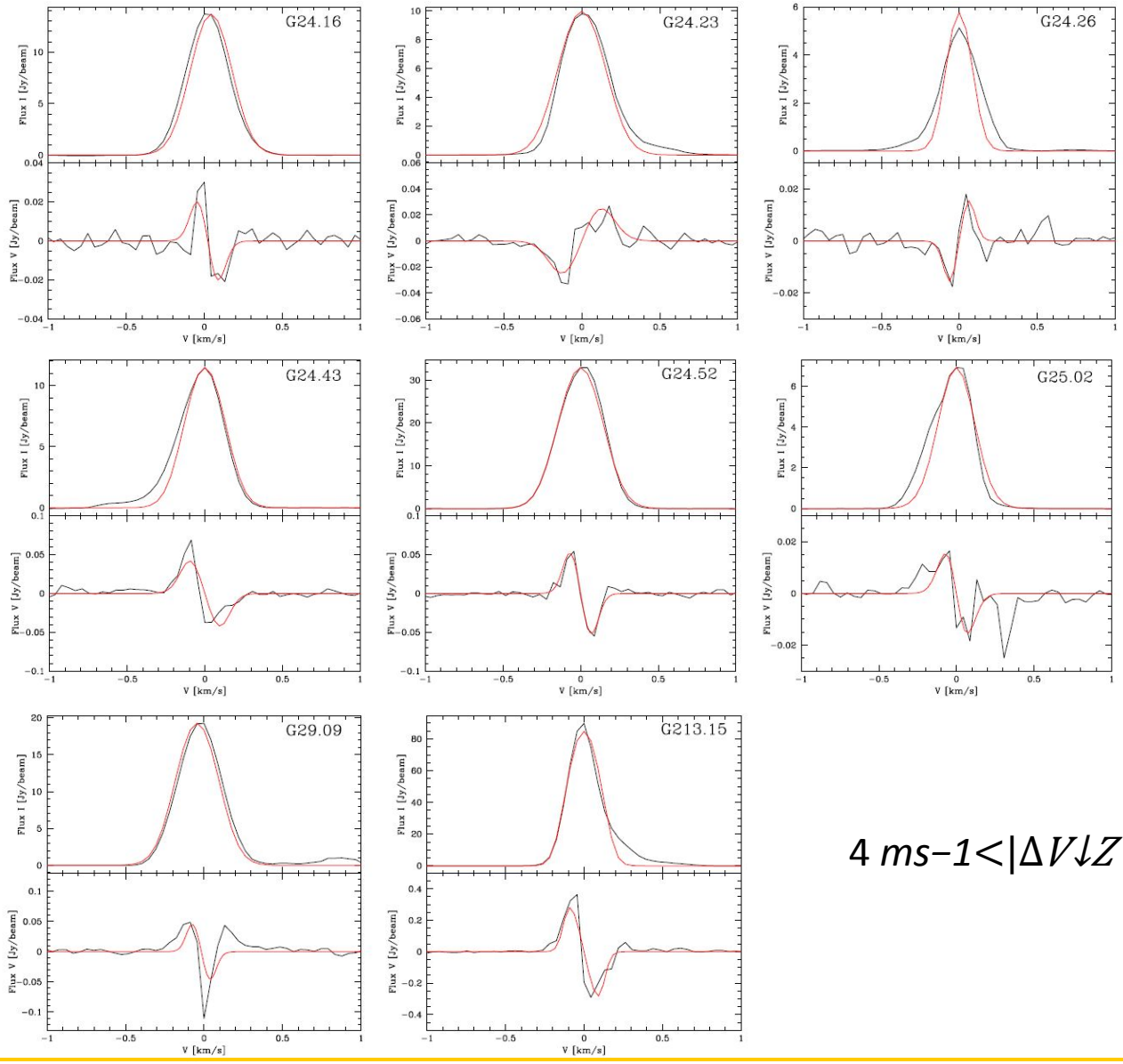

$4\ ms{-}1 < |\Delta V \downarrow Z| < 10\ ms^{-1}$

SOUL OF HIGH-MASS STAR FORMATION

EXTRA SLIDE 6

Foreground Faraday Rotation

$$\Phi[^\circ] = 4.22 \times 10^6 \, D[\mathrm{kpc}] \, n_e[\mathrm{cm}^{-3}] \, B_{||}[\mathrm{mG}] \, \nu^{-2}[\mathrm{GHz}]$$

W75N

where $n_e \approx 0.012$ cm^{-3} $B_{||} \approx 2 \times 10^{-3}$ mG $D = 1.3$ kpc

$\Phi_{water}[^\circ] \approx 0.3^\circ$ $\Phi_{meth}[^\circ] \approx 3.0^\circ$

EXTRA SLIDE 7

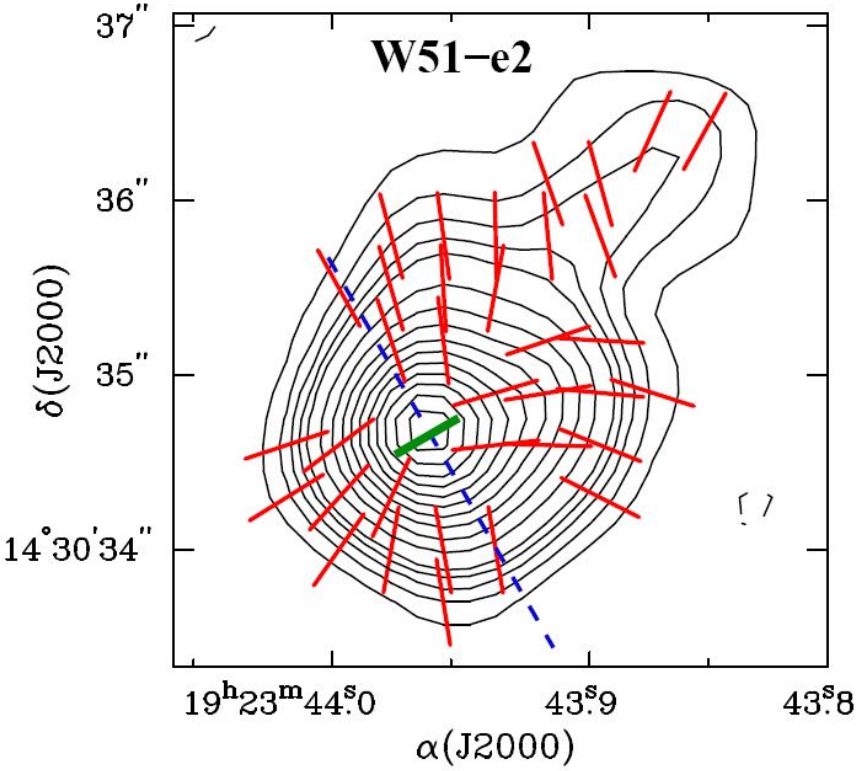

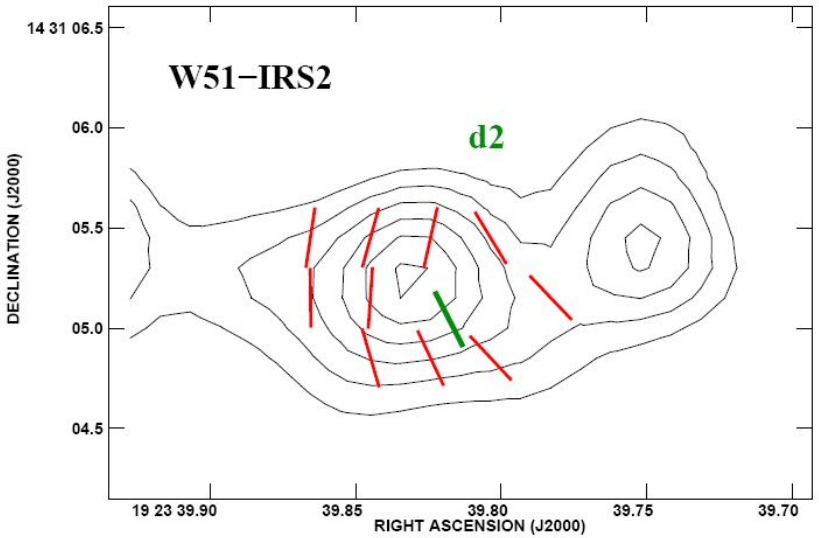

EXTRA SLIDE 8

Table 1: List of Targets and Status of the Observations.

Source name	RA (hh:mm:ss)	DEC (dd:mm:ss)	L_{bol} $L_\odot$	CH_3OH Flux (Jy)	H_2O Flux (Jy)	CH_3OH P.M., Pol.	H_2O P.M., Pol.	GST-time hours
G11.11−0.12P1	18:10:28.260	−19:22:30.30	$1 \cdot 10^3$	22	1	N, N	N, N	13–22
G012.68−0.18	18:13:54.750	−18:01:46.57	$5.7 \cdot 10^3$	300	500	N, N	Y, N	13–22
G012.91−0.26	18:14:39.510	−17:52:00.18	$2.7 \cdot 10^4$	317	5	N, N	Y, N	13–22
IRAS 18089−1732	18:11:51.390	−17:31:29.90	$3.2 \cdot 10^4$	7	75	N, N	N, N	13–22
G016.58−0.05	18:21:09.125	−14:31:48.65	$1.3 \cdot 10^4$	18	24	Y, N	Y, N	13–22
IRAS 18264−1152	18:29:14.360	−11:50:22.50	$1 \cdot 10^4$	4	50	N, N	N, N	13–22
G23.01−0.41	18:34:40.390	−09:00:38.50	$1 \cdot 10^5$	150	200	Y, Y	Y, N	13-22
G24.78+0.08	18:36:12.556	−07:12:10.80	$4 \cdot 10^4$	81	76	Y, Y	Y, N	13–22
G25.83−0.18	18:39:03.630	−06:24:11.20	$\leq 1.5 \cdot 10^5$	59	453	N, Y	N, N	13–22
G25.65+1.05	18:34:20.900	−05:59:42.10	$4.4 \cdot 10^4$	102	453	N, Y	N, N	13–22
G29.95−0.02	18:46:03.740	−02:39:22.33	$1.8 \cdot 10^4$	169	63	N, Y	N, N	13–22
G31.28+0.06	18:48:12.390	−01:26:22.60	$1.2 \cdot 10^5$	74	150	N, Y	N, N	13–22
G31.41+0.31	18:47:34.314	−01:12:45.80	$3 \cdot 10^5$	10	108	Y, N	Y, N	13–22
G35.20−0.74	18:58:12.980	+01:40:37.50	$1.6 \cdot 10^3$	200	16	N, Y	N, Y	13–22
G35.02+0.35	18:54:00.660	+02:01:18.55	$2.8 \cdot 10^4$	26	20	N, Y	Y, N	13–22
G37.43+1.51	18:54:14.229	+04:41:41.14	$1.3 \cdot 10^4$	349	110	N, Y	Y, N	13–22
G43.80−0.13	19:11:53.990	+09:35:50.30	$5 \cdot 10^4$	40	232	N, Y	N, N	13–22
G69.52−0.97	20:10:09.070	+31:31:34.40	$1.6 \cdot 10^4$	96	150	Y, Y	Y, N	16–01
G075.76+0.34	20:21:41.094	+37:25:29.19	$1.4 \cdot 10^4$	39	21	N, N	Y, N	16–01
G111.25−0.77	23:16:10.331	+59:55:28.63	$5 \cdot 10^3$	8	30	N, N	Y, N	17–02
Sh 2–255 IR	06:12:54.018	+17:59:23.12	$9 \cdot 10^3$	60	500	Y, Y	Y, N	01–10
G213.70−12.6	06:07:47.860	−06:22:56.63	$1.4 \cdot 10^4$	147	100	N, Y	N, N	01–10

Notes. Columns 1, 2–3 and 4 report the source name (in italic characters for maser associations identified with JVLA), (RA and DEC) coordinates, and bolometric luminosity, respectively; Columns 5 and 6 give the peak flux density of the 6.7 GHz CH_3OH and 22 GHz H_2O masers, respectively; Columns 7 and 8 report the status of the proper motion (P.M.) and polarization (Pol.) measurements for the CH_3OH and H_2O masers, respectively; Column 9 lists the GST time of the requested observations.